

Analysis of the Picard-Newton iteration for the Navier-Stokes equations: global stability and quadratic convergence

Sara Pollock^{*} Leo G. Rebholz[†] Xuemin Tu[‡] Mengying Xiao[§]

February 20, 2024

Abstract

We analyze and test a simple-to-implement two-step iteration for the incompressible Navier-Stokes equations that consists of first applying the Picard iteration and then applying the Newton iteration to the Picard output. We prove that this composition of Picard and Newton converges quadratically, and our analysis (which covers both the unique solution and non-unique solution cases) also suggests that this solver has a larger convergence basin than usual Newton because of the improved stability properties of Picard-Newton over Newton. Numerical tests show that Picard-Newton dramatically outperforms both the Picard and Newton iterations, especially as the Reynolds number increases. We also consider enhancing the Picard step with Anderson acceleration (AA), and find that the AAPicard-Newton iteration has even better convergence properties on several benchmark test problems.

1 Introduction

The Navier-Stokes equations (NSE) are widely used to model incompressible Newtonian fluid flow, which has applications across the spectrum of science and engineering. On a domain $\Omega \subset \mathbb{R}^d$, $d = 2, 3$, they take the form

$$\begin{cases} -\nu\Delta u + u \cdot \nabla u + \nabla p = f & \text{in } \Omega, \\ \nabla \cdot u = 0 & \text{in } \Omega, \\ u = 0 & \text{on } \partial\Omega, \end{cases} \quad (1.1)$$

where u is the velocity of fluid, p is the pressure, ν is the kinematic viscosity of the fluid, and f is an external forcing term. The parameter $Re := \frac{1}{\nu}$ represents the Reynolds number. While our study herein is restricted to nonlinear solvers for the steady system (1.1) with homogenous Dirichlet boundary conditions, the results are extendable to solving the time dependent NSE at a fixed time step in a temporal discretization, as well as nonhomogeneous mixed Dirichlet/Neumann boundary conditions.

^{*}Department of Mathematics, University of Florida, Gainesville, FL, 32611, s.pollock@ufl.edu; partially supported by NSF grant DMS-2011519

[†]School of Mathematical and Statistical Sciences, Clemson University, Clemson, SC, 29364, rebholz@clemson.edu; partially supported by NSF grant DMS-2011490.

[‡]Department of Mathematics, University of Kansas, Lawrence, KS, 66049, xuemin@ku.edu.

[§]Department of Mathematics and Statistics, University of West Florida, Pensacola, FL, 32514, mxiao@uwf.edu.

NSE solutions are used in simulation processes that can avoid costly physical experiments. However, solving the NSE can be very challenging, as the NSE are a notoriously hard nonlinear PDE for which analytical solutions are rarely available and numerical solvers often fail. The purpose of this paper is to develop and analyze a seemingly new numerical solver that is simple to implement, is free from parameters, and has better convergence properties than existing solvers.

Perhaps the most commonly used nonlinear iteration for solving (1.1) is the Picard iteration, which is given by (suppressing the weak formulation and boundary conditions for the moment)

$$\begin{aligned} -\nu\Delta u_{k+1} + u_k \cdot \nabla u_{k+1} + \nabla p_{k+1} &= f, \\ \nabla \cdot u_{k+1} &= 0. \end{aligned}$$

We will denote this iteration as a fixed point iteration via $u_{k+1} = g_P(u_k)$. This iteration is known to be globally stable, i.e. bounded for any initial iterate and problem data. Moreover, for sufficiently small problem data, then Picard is globally convergent with a linear convergence rate [11, 33].

If a good initial guess u_0 is available, then a faster alternative to the Picard iteration is the Newton iteration, which is given by [13, 18]

$$\begin{aligned} -\nu\Delta u_{k+1} + u_k \cdot \nabla u_{k+1} + u_{k+1} \cdot \nabla u_k + \nabla p_{k+1} &= f + u_k \cdot \nabla u_k, \\ \nabla \cdot u_{k+1} &= 0. \end{aligned}$$

We will denote this iteration as a fixed point iteration via $u_{k+1} = g_N(u_k)$. This iteration will converge quadratically for small data and for a sufficiently close initial guess [11, 25]. A common strategy for solving NSE has been to run a method with larger convergence radius than Newton such as Picard (or Anderson accelerated Picard [9, 33]) or damped Newton, and then switch over to Newton once the iterates get close enough to the solution [18].

Over the years, many variations of the Picard and Newton iterations for the NSE have been developed to improve solver robustness, efficiency, or both. For example, algorithms have been developed that eliminate or reduce the complexity of the linear solves and saddle point problems [10, 14, 35, 39] which provide overall more efficient algorithms if they do not increase the total number of nonlinear iterations. Continuation methods for the NSE can provide convergence for higher Reynolds numbers [1, 16]. Anderson acceleration (AA) or other extrapolation methods have been shown to improve convergence and robustness [33, 31]. Multilevel methods put most of the computations on the coarser levels [7, 15, 19, 21, 23, 24] and can be quite effective, as can defect correction approaches [19, 22], and there is a long list of other techniques can be effective in certain settings [14, 28]. Each of these methods have their drawbacks, whether it be complexity of the implementation, sensitivity to parameters, or inefficiency.

Herein we consider a simple-to-implement solver for the NSE that is a composition of these two well-known methods as a 2 step iteration which we call the Picard-Newton iteration. At step k , the iteration is defined by first performing a Picard iteration, and then second by performing a Newton iteration on the Picard output, i.e.

$$u_{k+1} = g_{PN}(u_k) = g_N(g_P(u_k)).$$

This solver is intended for use on problems where Newton will not converge, i.e. for higher Reynolds number problems (otherwise there is clearly extra unnecessary work coming from the Picard step), and the main idea is to combine the robustness of Picard with the convergence order of Newton. We note in particular the simplicity of the method and its implementation.

The general idea of composing solvers to take advantage of the good properties of each is well established, and is strongly related to the idea of nonlinear preconditioning - indeed here the Picard iteration can be considered a preconditioner for Newton. An excellent review paper of Brune et al [5] shows how effective composing solvers can be on a variety of problems. There are also many works on various combinations of the Picard and Newton methods for systems other than NSE, such as in imaging [43], periodic systems [27], optimization problems [34], and saturated flow problems [30], although none seem to use the simple-to-implement strategy we study herein.

The purpose of this paper is to analyze and test the Picard-Newton iteration for the NSE. The analysis is divided into two parts. First in the case of small data (sufficient for NSE solution uniqueness) we prove the Picard-Newton iteration is stable for any initial iterate (usual Newton is not), and quadratically convergent for a sufficiently close initial guess. Second, for general data where NSE solution uniqueness may not hold, we prove quadratic convergence for a sufficiently close initial guess; and, we show that since the Picard step is globally stable, Picard-Newton is less vulnerable to the blowup behavior common for Newton. Several numerical tests illustrate the effectiveness of Picard-Newton, and in particular we find excellent results for convergence at higher Reynolds numbers for 2D and 3D driven cavity. Lastly, we consider enhancing the Picard step with $m = 1$ AA, and show that AAPicard-Newton an even more robust and efficient solver than Picard-Newton.

This paper is arranged as follows. In section 2 we set notation and provide mathematical preliminaries for a smoother analysis to follow. Section 3 analyzes and tests the Picard-Newton iteration, and section 4 considers AAPicard-Newton. Conclusions and future directions are discussed in section 5.

2 Mathematical preliminaries

We consider an open connected set Ω , and denote the natural function spaces for the NSE by

$$Q := \{v \in L^2(\Omega) : \int_{\Omega} v \, dx = 0\}, \quad (2.1)$$

$$X := \{v \in H^1(\Omega) : v = 0 \text{ on } \partial\Omega\}, \quad (2.2)$$

$$V := \{v \in X : (\nabla \cdot v, q) = 0 \, \forall q \in Q\}. \quad (2.3)$$

The L^2 inner product and norm are denoted by (\cdot, \cdot) and $\|\cdot\|$, respectively. Without confusion, the notation (\cdot, \cdot) is also used to represent the duality between H^{-1} and X , and $\|\cdot\|_{-1}$ denotes the norm on H^{-1} .

Recall that the Poincare inequality holds on X : there exists a constant C_P dependent only on the domain satisfying

$$\|\phi\| \leq C_P \|\nabla\phi\| \text{ for all } \phi \in X. \quad (2.4)$$

We use the skew-symmetric form of the nonlinear term: for all $v, w, z \in X$,

$$b^*(v, w, z) = (v \cdot \nabla w, z) + \frac{1}{2}((\nabla \cdot v)w, z),$$

and note that similar results hold as those below will hold with other energy preserving formulations of the nonlinear term including rotational form and EMAC [12, 6, 29]. Note an important property

of b^* is that $b^*(u, v, v) = 0$ for all $u, v \in X$. If the first argument of b^* satisfies $\|\nabla \cdot v\| = 0$, then skew-symmetry is not needed (and has no effect). For $v \in V$, this is the case. However, when using certain finite element subspaces of X and Q (such as Taylor-Hood elements), it may happen that the discretely divergence free space does not yield completely divergence-free functions. Hence, to be general and cover all cases, we utilize skew-symmetry in our analysis.

The following inequality hold for b^* [20, 39]: there exists a constant M dependent only on the domain Ω such that

$$b^*(v, w, z) \leq M \|\nabla v\| \|\nabla w\| \|\nabla z\|. \quad (2.5)$$

2.1 NSE preliminaries

Written in terms of b^* , the weak form of the NSE (1.1) is given by: Find $u \in V$ satisfying

$$\nu(\nabla u, \nabla v) + b^*(u, u, v) = (f, v) \quad \forall v \in V. \quad (2.6)$$

It is well known that the weak steady NSE system (2.6) admits solutions for any $f \in H^{-1}(\Omega)$ and $\nu > 0$ [11, 20], and that any solution to (1.1) or (2.6) satisfies

$$\|\nabla u\| \leq \nu^{-1} \|f\|_{-1}. \quad (2.7)$$

A sufficient condition for uniqueness of solutions is that the data satisfy [11, 20]

$$\alpha := M\nu^{-2} \|f\|_{H^{-1}} < 1.$$

While $\alpha < 1$ is not a necessary condition for uniqueness, it is known that for large enough data (i.e. α large enough) that uniqueness breaks down [20] and the NSE will admit multiple solutions.

3 Convergence analysis of the Picard-Newton iteration

In this section we analyze stability and convergence results for the Picard-Newton iteration, and test it on several benchmark problems. First, under the NSE uniqueness condition $\alpha < 1$, we prove the method is globally stable (i.e. stable for any initial iterate) and for a sufficiently good initial iterate converges quadratically. For $\alpha > 1$, we can no longer prove global stability but only that the Picard step of Picard-Newton is stable. We are still able to prove quadratic convergence, provided the initial guess is sufficiently close to a nonsingular NSE solution.

We begin by stating the Picard-Newton iteration in weak form.

Algorithm 3.1 (Picard-Newton iteration). *The Picard-Newton iteration consists of applying the composition of the Newton and Picard iterations: $g_{PN} = g_N \circ g_P$, i.e.*

Step 1: Find $\hat{u}_{k+1} = g_P(u_k)$ by finding $\hat{u}_{k+1} \in V$ satisfying

$$\nu(\nabla \hat{u}_{k+1}, \nabla v) + b^*(u_k, \hat{u}_{k+1}, v) = (f, v) \quad \forall v \in V. \quad (3.1)$$

Step 2: Find $u_{k+1} = g_N(\hat{u}_{k+1})$ by finding $u_{k+1} \in V$ satisfying

$$\nu(\nabla u_{k+1}, \nabla v) + b^*(\hat{u}_{k+1}, u_{k+1}, v) + b^*(u_{k+1}, \hat{u}_{k+1}, v) - b^*(\hat{u}_{k+1}, \hat{u}_{k+1}, v) = (f, v) \quad \forall v \in V. \quad (3.2)$$

3.1 Analysis for the case of $\alpha < 1$

Here we analyze stability and then convergence of the Picard-Newton method. We first prove that the method is globally stable, i.e. bounded by data and independent of the initial iterate.

Lemma 3.1. *Under the uniqueness condition $\alpha < 1$, we have that Picard-Newton iteration is stable: for every k , it holds that*

$$\begin{aligned}\|\nabla\hat{u}_k\| &\leq \nu^{-1}\|f\|_{-1}, \\ \|\nabla u_k\| &\leq \frac{1 + \alpha\nu^{-1}}{1 - \alpha}\|f\|_{-1}.\end{aligned}$$

Remark 3.2. *Global stability for the usual Newton algorithm for NSE does not hold. For $\alpha < 1$, the stability of the Picard-Newton algorithm comes from the Picard step.*

Proof. We begin by proving Step 1 is stable. Taking $v = \hat{u}_{k+1}$ in (3.1) vanishes the nonlinear term and gives us

$$\nu\|\nabla\hat{u}_{k+1}\|^2 = (f, \hat{u}_{k+1}) \leq \|f\|_{-1}\|\nabla\hat{u}_{k+1}\|,$$

which reduces to

$$\|\nabla\hat{u}_{k+1}\| \leq \nu^{-1}\|f\|_{-1}. \quad (3.3)$$

Note that this holds for any $\alpha > 0$.

Next, we consider Step 2 and take $v = u_{k+1}$, which eliminates the first nonlinear term and gives

$$\nu\|\nabla u_{k+1}\|^2 = -b^*(u_{k+1}, \hat{u}_{k+1}, u_{k+1}) + b^*(\hat{u}_{k+1}, \hat{u}_{k+1}, u_{k+1}) + (f, u_{k+1}).$$

Applying the bound (2.5) on the nonlinear terms and handling the forcing term as in the Picard iteration yields

$$\nu\|\nabla u_{k+1}\|^2 = M\|\nabla u_{k+1}\|^2\|\nabla\hat{u}_{k+1}\| + M\|\nabla\hat{u}_{k+1}\|^2\|\nabla u_{k+1}\| + \|f\|_{-1}\|\nabla u_{k+1}\|.$$

Using the bound (3.3) and reducing gives us

$$\begin{aligned}\|\nabla u_{k+1}\|^2 &\leq M\nu^{-2}\|f\|_{-1}\|\nabla u_{k+1}\|^2 + M\nu^{-3}\|f\|_{-1}^2\|\nabla u_{k+1}\| + \|f\|_{-1}\|\nabla u_{k+1}\| \\ &= \alpha\|\nabla u_{k+1}\|^2 + \alpha\nu^{-1}\|f\|_{-1}\|\nabla u_{k+1}\| + \|f\|_{-1}\|\nabla u_{k+1}\|,\end{aligned}$$

and thus since $\alpha < 1$ is assumed,

$$\|\nabla u_{k+1}\| \leq \frac{1 + \alpha\nu^{-1}}{1 - \alpha}\|f\|_{-1}.$$

■

We now prove that the Picard-Newton iteration converges quadratically, provided a sufficiently good initial guess.

Theorem 3.1. *Under the uniqueness condition $\alpha < 1$, the Picard-Newton algorithm for the steady NSE converges quadratically provided the initial guess is sufficiently close to the NSE solution (2.6).*

Remark 3.3. *The theorem above requires a sufficiently close initial guess u_0 , and in particular a sufficient condition that comes from the proof is that*

$$\frac{M\nu^{-1}\alpha^2}{1-\alpha}\|\nabla(u-u_0)\| < 1.$$

This shows that as α gets smaller the convergence basin for the initial guess grows (and approaches all of X as $\alpha \rightarrow 0$).

With the typical guess of $u_0 = 0$, the condition reduces to

$$1 > \frac{M\nu^{-1}\alpha^2}{1-\alpha}\|\nabla(u-u_0)\| = \frac{M\nu^{-1}\alpha^2}{1-\alpha}\|\nabla u\|.$$

Since $\|\nabla u\| \leq \nu^{-1}\|f\|_{-1}$ by (2.7), this sufficient condition is implied by

$$1 > \frac{M\nu^{-2}\|f\|_{-1}\alpha^2}{1-\alpha} = \frac{\alpha^3}{1-\alpha} \iff 1-\alpha > \alpha^3.$$

Hence $\alpha < 0.682$ is a sufficient condition for Picard-Newton to converge quadratically when the initial guess is $u_0 = 0$. In our tests, this sufficient condition is quite pessimistic and we observe convergence even when $\alpha \gg 1$.

Proof of Theorem 3.1. Let u be the solution of (2.6), and denote $e_k = u - u_k$ and $\hat{e}_k = u - \hat{u}_k$. Since $u \in V$, we have $e_k, \hat{e}_k \in V$ as well.

To bound the error in Step 1, we subtract the Step 1 equation (3.1) from (2.6), which gives

$$\nu(\nabla\hat{e}_{k+1}, \nabla v) + b^*(u_k, \hat{e}_{k+1}, v) + b^*(e_k, u, v) = 0 \quad \forall v \in V.$$

Taking $v = \hat{e}_{k+1}$, the first nonlinear term vanishes and we obtain

$$\nu\|\nabla\hat{e}_{k+1}\|^2 = -b^*(e_k, u, \hat{e}_{k+1}) \leq M\|\nabla e_k\|\|\nabla u\|\|\nabla\hat{e}_{k+1}\| \leq M\nu^{-1}\|f\|_{-1}\|\nabla e_k\|\|\nabla\hat{e}_{k+1}\|,$$

thanks to the bound (2.5) on b^* and (2.7). Multiplying both sides by ν^{-1} , using the definition of α and reducing, we get the bound

$$\|\nabla\hat{e}_{k+1}\| \leq \alpha\|\nabla e_k\|. \quad (3.4)$$

Next, subtract Step 2 (3.2) from (2.6), term by term, which yields

$$\nu(\nabla e_{k+1}, \nabla v) + b^*(\hat{u}_{k+1}, e_{k+1}, v) + b^*(e_{k+1}, \hat{u}_{k+1}, v) - b^*(\hat{e}_{k+1}, \hat{e}_{k+1}, v) = 0 \quad \forall v \in V, \quad (3.5)$$

noting that we used the identities $b^*(u, u, v) - b^*(\phi, \chi, v) = b^*(u - \phi, \chi, v) + b^*(u, u - \chi, v)$ and $b^*(u, u, v) - b^*(\phi, \chi, v) = b^*(u, u - \chi, v) + b^*(u - \phi, \chi, v)$ on the three nonlinear term differences. Taking $v = e_{k+1}$ vanishes the second term, leaving

$$\begin{aligned} \nu\|\nabla e_{k+1}\|^2 &= -b^*(e_{k+1}, \hat{u}_{k+1}, e_{k+1}) + b^*(\hat{e}_{k+1}, \hat{e}_{k+1}, e_{k+1}) \\ &\leq M\|\nabla e_{k+1}\|^2\|\nabla\hat{u}_{k+1}\| + M\|\nabla\hat{e}_{k+1}\|^2\|\nabla e_{k+1}\|, \end{aligned}$$

with the last step thanks to (2.5). Now using (3.3) and (3.4) and the definition of α , we obtain

$$\|\nabla e_{k+1}\| \leq \alpha\|\nabla e_{k+1}\| + M\nu^{-1}\|\nabla\hat{e}_{k+1}\|^2 \leq \alpha\|\nabla e_{k+1}\| + M\nu^{-1}\alpha^2\|\nabla e_k\|^2,$$

which reduces to

$$\|\nabla e_{k+1}\| \leq \frac{M\nu^{-1}\alpha^2}{1-\alpha} \|\nabla e_k\|^2$$

and proves asymptotic quadratic convergence provided the sequence of iterates converges. A sufficient condition for this is that e_0 satisfies

$$\frac{M\nu^{-1}\alpha^2}{1-\alpha} \|\nabla e_0\| < 1.$$

This can be satisfied with u_0 being sufficiently close to u , and how close it needs to be depends on the size of α .

■

A somewhat sharper analysis than is given above which could allow for larger α comes from a sharper estimate of the nonlinear term. A key estimate used in the proofs above is (2.5), which we recall the proof from [11, 20] comes from Hölder and Sobolev embeddings and first shows

$$b^*(z, w, v) \leq M_0 \|z\|^{1/2} \|\nabla z\|^{1/2} \|\nabla w\| \|\nabla v\|, \quad (3.6)$$

and then applies the Poincaré inequality (2.4) to obtain

$$b^*(z, w, v) \leq M \|\nabla z\| \|\nabla w\| \|\nabla v\|,$$

where $M = C_P^{1/2} M_0$. Hence to get a sharper estimate, we can back up one step to (3.6) to obtain

$$b^*(z, w, v) \leq \frac{M}{C_P^{1/2}} \left(\frac{\|z\|}{\|\nabla z\|} \right)^{1/2} \|\nabla z\| \|\nabla w\| \|\nabla v\|. \quad (3.7)$$

The main advantage of the bound (3.6) over (3.7) is that for complex flows we expect $\|u\| \ll \|\nabla u\|$, (i.e. vorticity is more complex than velocity) hence the term $\left(\frac{\|z\|}{\|\nabla z\|} \right)^{1/2}$ can in practice be small. In all of our numerical tests herein, the ratio $\left(\frac{\|u\|}{\|\nabla u\|} \right)^{1/2}$ is never larger than 0.2. Hence if the iteration is close to the root, then we expect similar size ratios for $z = u, u_{k+1}, \hat{u}_{k+1}, e_{k+1}$, and \hat{e}_{k+1} . This helps explain why we often in practice see convergence behavior in the regime where $\alpha > 1$ that agrees with the above analysis even though the restrictive data condition is not met. In the next section we consider further what can be shown if $\alpha < 1$ does not hold.

3.2 The case of large problem data

The proofs above for global stability and convergence of the Picard-Newton iteration no longer hold when $\alpha \geq 1$. Moreover, classical convergence proofs of the usual Picard iteration and usual Newton iteration (see e.g. [18, 11]) also no longer hold. Still, convergence of the Picard and Newton iterations for larger data has been shown in many applications, and so we consider this important case also. We are able to prove for any $\alpha > 1$ that Picard-Newton is locally quadratically convergent to a nonsingular NSE solution.

We begin by recalling from [20, Chapter 6.4] that isolated nonsingular solutions of the NSE exist for any $\alpha > 0$. For an isolated solution, there exists some positive r so that a ball radius

r around that solution contains no other NSE solution. Moreover, if u^* is a nonsingular solution, then there exists $\delta > 0$ depending on Ω, ν, u^* such that for any $w \in V$,

$$\sup_{0 \neq v \in V} \frac{\nu(\nabla w, \nabla v) + b^*(u^*, w, v) + b^*(w, u^*, v)}{\|\nabla v\|} \geq \delta \|\nabla w\|. \quad (3.8)$$

This property for nonsingular solutions is key to proving the following local convergence result, which holds for any $\alpha > 0$. We note that the proof of the theorem requires the initial guess to be good enough, and as the Reynolds number grows the basin of convergence gets smaller. We restrict our stability analysis to this basin of convergence. However, the Picard step is globally stable so if unstable growth occurs at a Newton step, the growth is automatically controlled by the globally bounded Picard step that follows. In other words, since the stability at the half step is guaranteed, the Newton step is always applied with an input velocity that is bounded, and can not be part of a sequence of iterates that is blowing up.

Theorem 3.4 (Local convergence to nonsingular solutions for any problem data). *Let u be a nonsingular steady NSE solution for given data f, ν, Ω . Then for an initial guess sufficiently close to u , the Picard-Newton iteration converges quadratically to u .*

Proof. We recall from the convergence proof in the $\alpha < 1$ case that (3.4) holds for any $\alpha > 0$:

$$\|\nabla \hat{e}_{k+1}\| \leq \alpha \|\nabla e_k\|.$$

To analyze the Newton step, we proceed just as for (3.5), which states

$$\nu(\nabla e_{k+1}, \nabla v) = -b^*(\hat{u}_{k+1}, e_{k+1}, v) - b^*(e_{k+1}, \hat{u}_{k+1}, v) + b^*(\hat{e}_{k+1}, \hat{e}_{k+1}, v) \quad \forall v \in V.$$

Adding $b^*(u, e_{k+1}, v)$ and $b^*(e_{k+1}, u, v)$ to both sides yields

$$\begin{aligned} \nu(\nabla e_{k+1}, \nabla v) + b^*(u, e_{k+1}, v) + b^*(e_{k+1}, u, v) = \\ b^*(\hat{e}_{k+1}, e_{k+1}, v) + b^*(e_{k+1}, \hat{e}_{k+1}, v) + b^*(\hat{e}_{k+1}, \hat{e}_{k+1}, v) \quad \forall v \in V. \end{aligned}$$

We now divide both sides by (nonzero) $\|\nabla v\|$, then majorize the right hand side using (2.5) and then take the supremum over nonzero $v \in V$:

$$\sup_{0 \neq v \in V} \frac{\nu(\nabla e_{k+1}, \nabla v) + b^*(u, e_{k+1}, v) + b^*(e_{k+1}, u, v)}{\|\nabla v\|} \leq 2M \|\nabla \hat{e}_{k+1}\| \|\nabla e_{k+1}\| + M \|\nabla \hat{e}_{k+1}\|^2.$$

Thus by (3.8) since u is nonsingular we can lower bound the left hand side to get

$$\begin{aligned} \delta \|\nabla e_{k+1}\| &\leq 2M \|\nabla \hat{e}_{k+1}\| \|\nabla e_{k+1}\| + M \|\nabla \hat{e}_{k+1}\|^2 \\ &\leq 2M\alpha \|\nabla e_k\| \|\nabla e_{k+1}\| + M\alpha^2 \|\nabla e_k\|^2, \end{aligned}$$

thanks to (3.4). For $\|\nabla e_k\|$ sufficiently small, this reduces to

$$(\delta - 2M\alpha \|\nabla e_k\|) \|\nabla e_{k+1}\| \leq M\alpha^2 \|\nabla e_k\|^2. \quad (3.9)$$

From here, the assumption of a good enough initial guess is sufficient to imply quadratic convergence. To be precise, define $\lambda_k = \delta - 2M\alpha\|\nabla(u - u_k)\|$, and notice that $\lambda_k > \lambda_j$ whenever $\|\nabla e_k\| < \|\nabla e_j\|$. Then for an initial iterate u_0 that satisfies

$$\lambda_0 > 0 \quad \text{and} \quad \frac{M\alpha^2}{\lambda_0} \|\nabla(u - u_0)\| < 1, \quad (3.10)$$

each subsequent iterate satisfies

$$\|\nabla e_{k+1}\| \leq \frac{M\alpha^2}{\lambda_k} \|\nabla e_k\|^2 \leq \frac{M\alpha^2}{\lambda_0} \|\nabla e_k\|^2 \leq \frac{M\alpha^2}{\lambda_0} \|\nabla e_0\| \|\nabla e_k\|, \quad k \geq 0, \quad (3.11)$$

courtesy of (3.9), by which the iteration converges at least linearly, and in fact quadratically. ■

Remark 3.5. *More generally, it does not necessarily have to be the initial iterate u_0 that is sufficiently close to u . Rather, if some iterate u_J satisfies (3.10), namely*

$$\lambda_J > 0 \quad \text{and} \quad \frac{M\alpha^2}{\lambda_J} \|\nabla(u - u_J)\| < 1,$$

then (3.11) holds for each $k \geq J$ rather than each $k \geq 0$. This is particularly important in light of the previously noted boundedness of each Picard step, as we notice in practice that the iteration may produce a sequence of bounded (at each Picard half-step) then non-converging Newton iterates before falling into the basin of convergence. This combination of the Picard iterates preventing the Newton iterates from sequentially blowing up in the preasymptotic regime, followed by the quadratic convergence from the Newton iterates in the asymptotic regime, gives this two-step iteration an attractive combination of robustness and efficiency.

3.3 Numerical tests for Picard-Newton

We give here results from three numerical tests with Picard-Newton. They show that the method has good stability properties, converges quadratically, and is able to converge for much higher Reynolds numbers for the driven cavity problems than usual Picard or Newton. Scott-Vogelius conforming finite elements are used for all of our tests, with velocity-pressure pairs $(X_h, Q_h) = (P_k, P_{k-1}^{disc}) \cap (X, Q)$ and $k = d$. The meshes are constructed as simplexes, with barycenter refinements (a.k.a. Alfeld split in the Guzmán-Neilan vernacular) as the final step of the mesh construction in order to satisfy the LBB condition [2, 44].

For the 2D tests, the linear systems that arise at each step of Picard and Newton are solved with a direct solver. In 3D, we use GMRESM as the outer solver, and to precondition we follow the ideas of [3, 17] and add grad-div stabilization with parameter 100 (which has no effect on solution since we use divergence-free elements) and precondition the Schur complement with the pressure mass matrix. We perform the inner solves directly. This is a very effective solver, and typically it converges in less than 5 iterations with tolerance 10^{-8} for both Picard and for Newton. We tested changing the tolerance for Picard linear solvers to 10^{-3} (to make the preconditioner less computationally expensive), and it made almost no difference in the convergence of the nonlinear solver.

3.3.1 Analytical test

For our first numerical test, we illustrate the theory above in that Picard-Newton converges quadratically and will have a larger convergence basin than usual Newton. We consider solving the steady NSE with exact solution

$$u_{nse} = \begin{pmatrix} \cos(x) \sin(y) \\ -\sin(x) \cos(y) \end{pmatrix}, \quad p_{nse} = -\frac{1}{4}(\cos(2x) + \cos(2y)) + x + y,$$

over a unit square Ω and with Reynolds number $Re = 1/\nu = 1000$. We calculate f from the NSE and chosen solution and ν . Nonhomogenous boundary conditions are used in the tests, and the true solution is used as the boundary condition. Tests are run for the Picard iteration, the Newton iteration, and the proposed Picard-Newton iteration, with varying initial guesses.

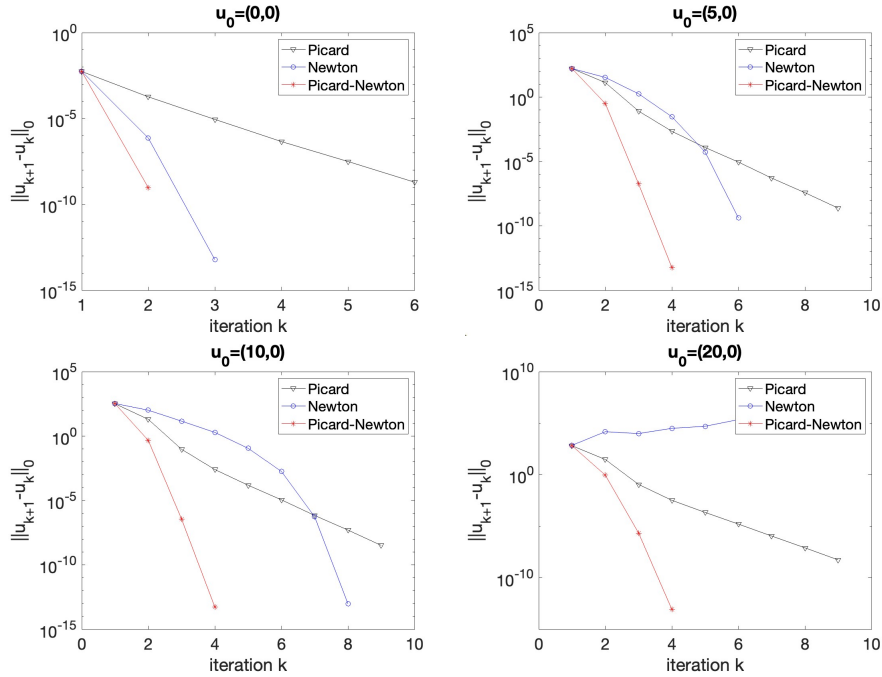


Figure 1: Convergence plots of the analytical test with various initial values $u_0 = (c, 0)^T, c = 0, 1, 5, 10, 20$.

For computations, we partition the domain into a barycenter refinement of a uniform triangular mesh with maximum diameter $h = 1/32$, choose (P_2, P_1^{dc}) Scott-Vogelius elements, and set the convergence tolerance for the iterative methods (Picard, Newton and Picard-Newton) to be $tol = 10^{-8}$ in the L^2 norm.

$$u_0 = \begin{pmatrix} c \\ 0 \end{pmatrix} \text{ in } \Omega, \quad u_0 = u_{ex} \text{ on } \partial\Omega,$$

with $c = 0, 5, 10$, and 20 .

Convergence results are shown in figure 1 for each of the different initial guesses. We observe linear convergence of Picard in all tests, and superlinear convergence for Newton (when it converged) and Picard-Newton always converging faster than Newton. However, Newton failed to converge

for the largest initial guess. We note that we checked that all solutions found by the solvers were accurate to within 10^{-4} in the L^2 norm, which is approximately the optimal accuracy one can expect from interpolation on this mesh.

3.3.2 2D driven cavity

For our next test we consider Picard-Newton applied to the 2D driven cavity benchmark problem. The domain is the unit square $\Omega = (0, 1)^2$, and we compute with (P_2, P_1^{disc}) Scott-Vogelius elements on a barycenter refined uniform triangular meshes. We use $f = 0$ and Dirichlet boundary conditions that enforce no-slip velocity on the sides and bottom, and $\langle 1, 0 \rangle^T$ on the top (lid). In this problem $Re := \nu^{-1}$. A plot of the velocity solutions found on the barycenter refined $h = \frac{1}{128}$ mesh (394K velocity degrees of freedom (dof), 294K pressure dof) for varying Re are shown in figure 2, and these compare well with the literature [8]. We note that the initial guess is $u_0 = 0$, and no continuation or acceleration methods are used here.

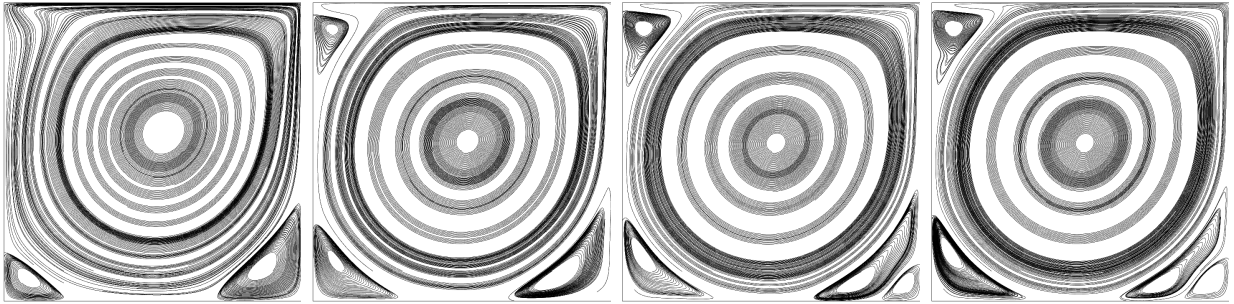


Figure 2: Shown above are streamlines of velocity solutions found for the 2D driven cavity problems with $Re=1000, 5000, 10000$, and 12000 (from top left to bottom right).

We run tests with $Re=1000, 2500, 5000, 10000$ and 12000 , on meshes constructed as barycenter refinements of uniform triangulations with $h = \frac{1}{32}, \frac{1}{64}, \frac{1}{128}$ and $\frac{1}{196}$, which provided 42K, 170K, 688K, and 1.6M dof respectively. Convergence results are shown in figure 3 as plots of the fixed point residuals (i.e. difference in successive iterates) in the H^1 norm, and we observe quadratic convergence in all cases except for $Re=12000$ on the finest mesh, which fails. The convergence for $Re \leq 2500$ appears to be mesh independent, which our analysis proves is the case for small data. However, for $Re \geq 5000$, we observe that convergence is slower on each successive mesh, e.g. for $Re=10000$ the number of iterations to converge on the successively finer meshes is 6, 23, 52 and 56. For these higher Re , we observe residual values stayed stable but did not decrease in the early iterations, before finally converging.

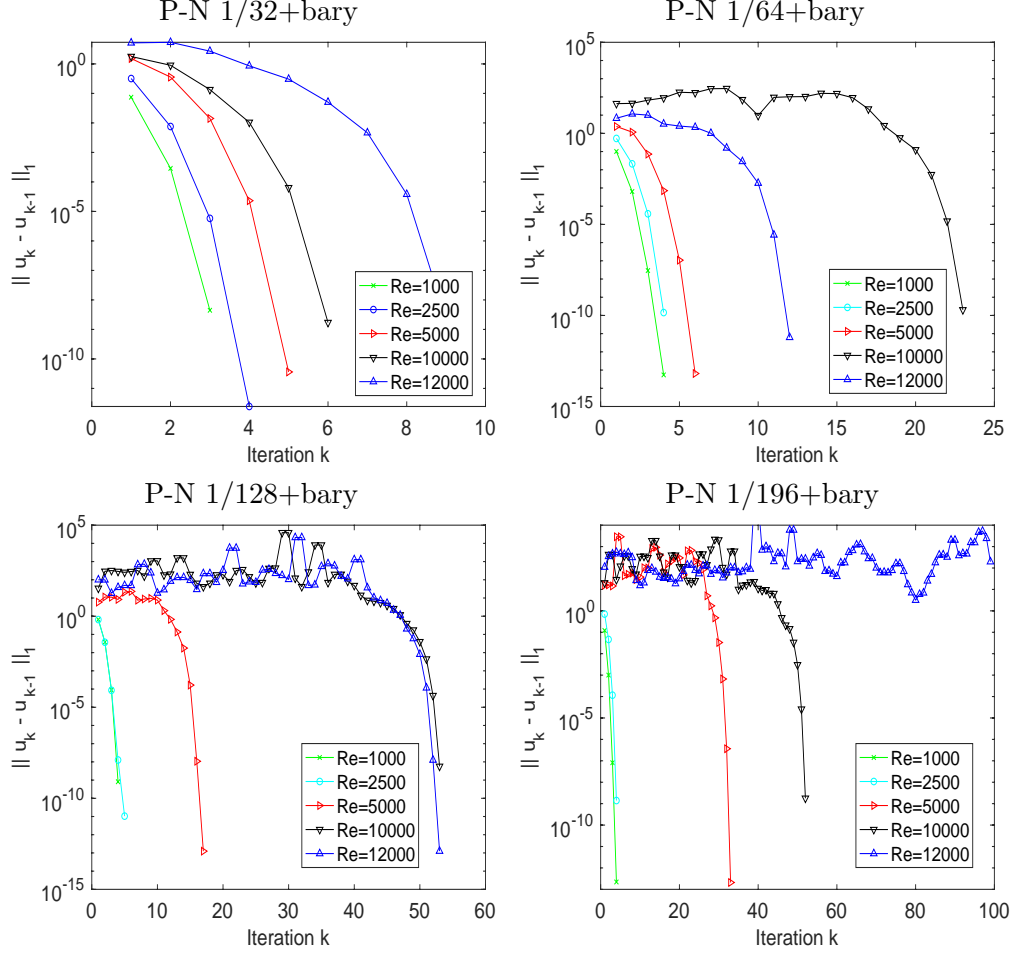


Figure 3: Shown above are convergence plots for the Picard-Newton iteration for varying Re , for meshes using $h = \frac{1}{32}$, $h = \frac{1}{64}$, $h = \frac{1}{128}$ and $h = \frac{1}{196}$ before barycenter refinement.

For comparison, in figure 4 we show convergence plots for Picard, Newton and Newton with Line Search (NLS) for varying Re on the barycenter refined $h = \frac{1}{64}$ mesh. Here we observe that Picard will converge for roughly $Re \leq 4000$, Newton will converge for roughly $Re \leq 2500$ and Newton with line search will converge for roughly $Re \leq 3000$ (the line search implementation checks for a decrease in the nonlinear NSE finite element residual vector for a given step size, and if no decrease is found then the step size is cut in half, to a minimum of $\frac{1}{32}$ step size). Hence it is clear the proposed Picard-Newton method is able to converge for much higher Reynolds number than Picard, Newton, or Newton with line search are able to.

3.3.3 3D driven cavity

Our next test is for the 3D lid-driven cavity benchmark problem, which is a 3D analogue of the 2D cavity test problem above. The domain is the unit cube, there is no forcing ($f = 0$), homogeneous Dirichlet boundary conditions are enforced on the walls except that $u = \langle 1, 0, 0 \rangle$ at the top of the box to represent the moving lid. The viscosity is chosen as the inverse of the Reynolds number, and we will use several choices of Re .

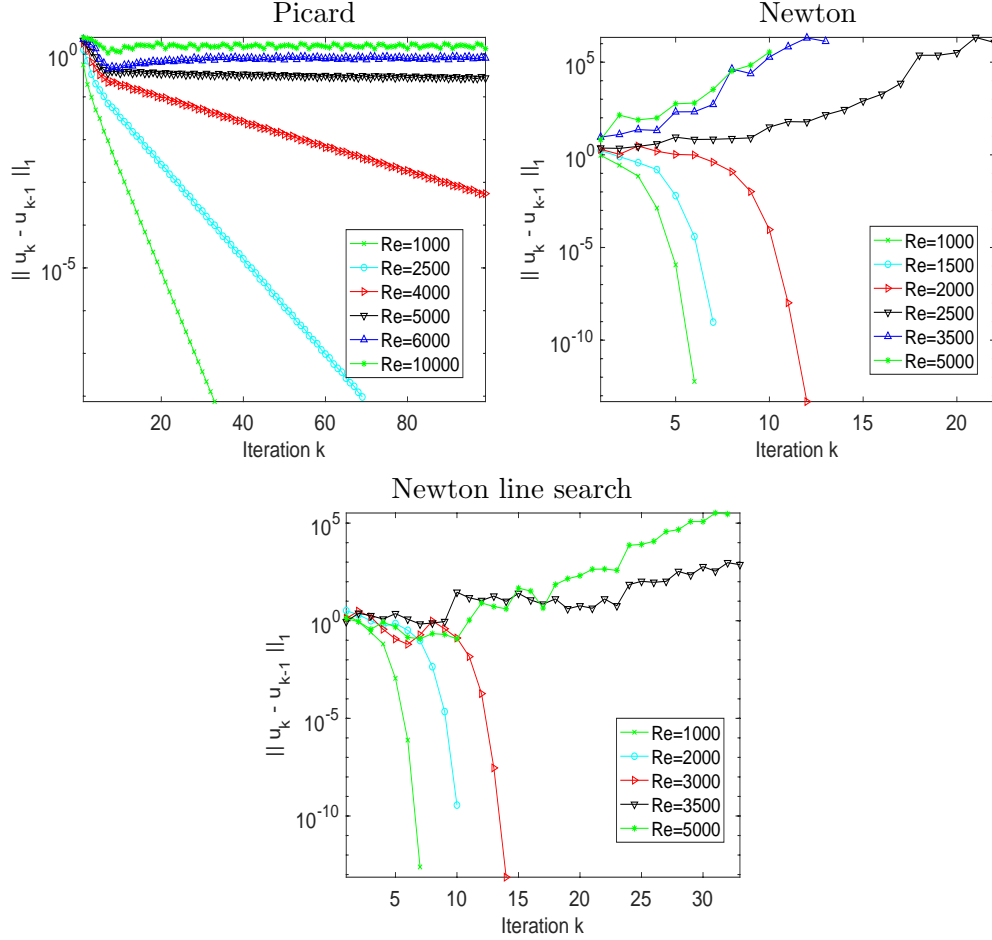


Figure 4: Shown above are convergence plots for the Picard (top left), Newton (top right) and Line Search Newton (bottom center), all using varying Re , but all using a barycenter refined $h = \frac{1}{64}$ mesh.

We compute using two different meshes, which are constructed by first using Chebychev points on $[0,1]$ to construct $\mathcal{M} \times \mathcal{M} \times \mathcal{M}$ grids of rectangular boxes (we use $\mathcal{M}=8$ for mesh 1, 12 for mesh 2 and $\mathcal{M}=14$ for mesh 3). Each box is then split into 6 tetrahedra via the splitting shown in 5, and then each of these tetrahedra is split into 4 tetrahedra with a barycenter refinement. The mesh is then equipped with (P_3, P_2^{disc}) Scott-Vogelius elements, and this provides for approximately 206K total dof for mesh 1, 796K total dof for mesh 2, and 1.3 million total dof for mesh 3. Solution plots found with this discretization matched those from the literature [41], and we show the midsplceplanes of the $Re=1000$ mesh 2 solution in figure 6.

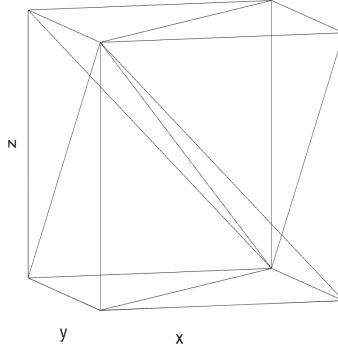


Figure 5: Shown above is the method used to split a rectangular box into 6 tetrahedra.

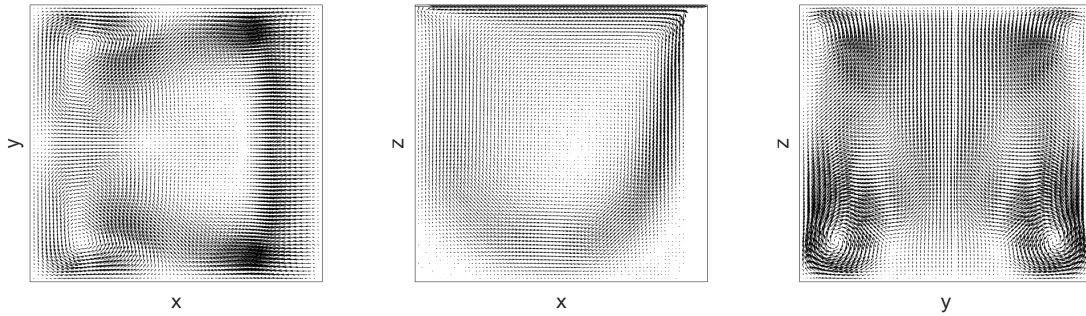


Figure 6: Shown above are mid-sliceplanes of the solution for the 3D driven cavity simulations at $Re=1000$.

We test convergence for the Newton, Picard, and Picard-Newton iterations for varying Re , and on all three meshes, always using $u_0 = 0$ for the initial iterate. For each case, we test how many iterations it takes for the residual to drop below 10^{-8} in the H^1 norm. We consider failure to be lack of convergence within 200 iterations, and we call it blowup if the L^2 residual ever grows above 10^4 , (and when this happens our linear solvers fail). Convergence results are shown in table 1. As expected, Newton and Picard iterations only converge for smaller Re . Picard-Newton, on the other hand, is able to converge for much larger Re , up to $Re = 1800$ on mesh 3. We note this is without any acceleration methods, continuation methods, line search, or other; it is simply the two step Picard-Newton iteration. We note that the results suggest some mesh independence of the convergence: up to $Re = 1400$, the number of iterates to convergence for Picard-Newton is about the same on meshes 2 and 3. Interestingly, convergence for $Re=1600$ and 1800 is achieved on mesh 3 but not on mesh 1 or mesh 2.

	Mesh 1			Mesh 2			Mesh 3		
Re / method	Newt	Pic	P-N	Newt	Pic	P-N	Newt	Pic	P-N
100	6	30	4	5	26	4	5	26	4
200	7	121	5	6	180	5	6	185	5
400	8	F	6	8	F	6	8	F	6
600	11	F	7	14	F	7	B	F	7
800	B	F	7	B	F	9	B	F	9
1000	B	F	9	B	F	11	B	F	13
1200	B	F	10	B	F	12	B	F	13
1400	B	F	10	B	F	34	B	F	33
1600	B	F	11	B	F	F	B	F	68
1800	B	F	11	B	F	F	B	F	176
2000	B	F	13	B	F	F	B	F	F

Table 1: Shown above are convergence results (number of iterations, ‘F’ if no convergence after 200 iterations, ‘B’ if H^1 residual grows above 10^4) for the Picard, Newton and Picard-Newton iterations for varying Re and on mesh 1 and mesh 2.

4 Anderson accelerated Picard-Newton

Anderson acceleration (AA) has recently been shown to be very effective at accelerating and enabling convergence of fixed point methods, and in particular for the Picard method for the NSE [33, 9, 31]. Hence it seems appropriate to test if AA can also help improve convergence in the Picard-Newton iteration. There are multiple ways AA could be applied: to the Picard iteration g_P , to the Newton iteration g_N , to the entire iteration g_{PN} , and combinations thereof. In light of the recent work of [42, 36] where it was shown that AA reduces the asymptotic convergence order of superlinearly converging methods including for the NSE, we focus here on applying AA only to the Picard step (but we note that we did see modest improvement with AA applied to the g_{PN} ; results omitted). For simplicity, we consider only the case of depth $m = 1$ and no relaxation for these initial tests, but remark that further improvement is very likely possible with optimal depth and relaxation parameters. Hence for the proposed AAPicard-Newton solver studied in this section, each iteration will require two Picard solves and one Newton solve at each iteration.

4.1 AA background

The Anderson acceleration algorithm is defined as follows. For a fixed point function $g : X \rightarrow X$ with X a Hilbert space with norm $\|\cdot\|_X$, the depth $m \geq 0$ AA algorithm with damping parameters $0 < \beta_{k+1} \leq 1$ is given by:

Step 0: Choose $x_0 \in X$.

Step 1: Find $w_1 \in X$ such that $w_1 = g(x_0) - x_0$. Set $x_1 = x_0 + w_1$.

Step $k + 1$: For $k = 1, 2, 3, \dots$ Set $m_k = \min\{k, m\}$.

[a.] Find $w_{k+1} = g(x_k) - x_k$.

[b.] Solve the minimization problem for $\{\alpha_j^{k+1}\}_{j=k-m_k}^k$

$$\min_{\sum_{j=k-m_k}^k \alpha_j^{k+1} = 1} \left\| \sum_{j=k-m_k}^k \alpha_j^{k+1} w_{j+1} \right\|_X \quad (4.1)$$

[c.] For a selected damping factor $0 < \beta_{k+1} \leq 1$, set

$$x_{k+1} = \sum_{j=k-m_k}^k \alpha_j^{k+1} x_j + \beta_{k+1} \sum_{j=k-m_k}^k \alpha_j^{k+1} w_{j+1}, \quad (4.2)$$

where $w_{k+1} := g(x_k) - x_k$ represents the stage k residual.

Remark 4.1. *The convergence theory assumes the α_j^{k+1} are uniformly bounded. As discussed in [31, 32], this is equivalent to assuming full column rank of the matrix with columns $(w_{j+1} - w_j)_{j=k, k-1, \dots, k-m}$ and can be controlled by length and angle filtering.*

A key idea of [33, 31] in understanding how AA improves linearly convergent methods was to define the gain of the optimization problem by

$$\theta_k := \frac{\left\| \sum_{j=k-m_k}^k \alpha_j^{k+1} w_{j+1} \right\|_X}{\|w_k\|_X}. \quad (4.3)$$

This is considered the gain factor because the numerator represents the minimum value of the sum using the optimal parameters, while the denominator is the value of the sum if the usual fixed point method was used. With this, it can be proven that AA improves the linear convergence rate by scaling it by the gain factor θ_k of the underlying AA optimization problem [33, 9, 31]. For AA depth $m = 1$, the result from Theorem 4.1 in [31] reads

$$\begin{aligned} \|w_{k+1}\|_X &\leq \|w_k\|_X \left\{ \theta_k \left((1 - \beta_k) + \kappa_g \beta_k \right) + \hat{\kappa}_g \sigma^{-1} \sqrt{1 - \theta_k^2} \right. \\ &\times \left. \left(\|w_k\|_X \left(\sigma^{-1} \sqrt{1 - \theta_k^2} + \beta_k \theta_k \right) + \|w_{k-1}\|_X \left(\sigma^{-1} \sqrt{1 - \theta_{k-1}^2} + \beta_{k-1} \theta_{k-1} \right) \right) \right\}, \end{aligned} \quad (4.4)$$

where κ_g is the linear convergence rate of the usual fixed point iteration, $\hat{\kappa}_g$ is the Lipschitz constant of g' , and $\sigma > 0$ satisfies

$$\|w_{k+1} - w_k\|_X \geq \sigma \|x_k - x_{k-1}\|_X. \quad (4.5)$$

The above result assumes $\sigma > 0 \forall k$ and g is Lipschitz continuously differentiable, and we note that if g is contractive then $\sigma = 1 - \kappa_g$ ([31] discusses the case when g is not contractive).

Remark 4.2. *Equation 4.4 also reveals whether the mesh size h affects the convergence. For the NSE, the Lipschitz constant κ_g is independent of h [33]. We observe very little difference in the convergent plots for various h in our tests. However, for certain fluid models, such as Bingham viscoplastic model, the Lipschitz constant κ_g has a negative scaling with h , see Lemma 3.5 in [26].*

4.2 Numerical Tests for AAPicard-Newton

We now give results for three numerical tests for AAPicard-Newton, with focus on how it improves over Picard-Newton. For the AA, we use only depth $m = 1$ and no relaxation. We use the same linear solvers as in the tests above for Picard-Newton.

Algorithm 4.3 (AAPicard-Newton with $m = 1$ and no relaxation). *The AAPicard-Newton iteration with Anderson depth $m = 1$ and no relaxation consists of applying the composition of the Newton and Anderson accelerated Picard iterations for solving Navier-Stokes equations: $g_N \circ g_{AP}$, i.e.,*

Step 1: Find $\tilde{u}_{k+1} = g_P(u_k)$ by finding $\tilde{u}_{k+1} \in V$ satisfying

$$\nu(\nabla\tilde{u}_{k+1}, \nabla v) + b^*(u_k, \tilde{u}_{k+1}, v) = (f, v) \quad \forall v \in V. \quad (4.6)$$

Step 2: Find $\tilde{\tilde{u}}_{k+1} = g_P(\tilde{u}_{k+1})$ by finding $\tilde{\tilde{u}}_{k+1} \in V$ satisfying

$$\nu(\nabla\tilde{\tilde{u}}_{k+1}, \nabla v) + b^*(\tilde{u}_{k+1}, \tilde{\tilde{u}}_{k+1}, v) = (f, v) \quad \forall v \in V. \quad (4.7)$$

Step 3: Determine α^{k+1} by

$$\alpha^{k+1} = \frac{(\nabla\tilde{\tilde{u}}_{k+1}, \nabla(\tilde{\tilde{u}}_{k+1} - \tilde{u}_{k+1}))}{\|\nabla(\tilde{\tilde{u}}_{k+1} - \tilde{u}_{k+1})\|^2}$$

and set

$$\hat{u}_{k+1} = (1 - \alpha^{k+1})\tilde{\tilde{u}}_{k+1} + \alpha^{k+1}\tilde{u}_{k+1}.$$

Step 4: Find $u_{k+1} = g_N(\hat{u}_{k+1})$ by finding $u_{k+1} \in V$ satisfying (3.2).

4.2.1 2D Driven Cavity

We now test AAPicard-Newton on the 2D driven cavity problem (same setup as above) with $Re=10000, 12000, 15000, 20000,$ and 25000 , first with a barycenter refined $h = \frac{1}{128}$ uniform triangulation and also a barycenter refined $h = \frac{1}{196}$ uniform triangulation. Plots of solutions for the $Re=10000, 15000, 20000$ and 25000 that were found on the $h = \frac{1}{196}$ mesh are shown in figure 7. These plots match those found in [8] quite well, although 25000 is beyond what is reported in their paper. We note that no relaxation or continuation methods are used to get these results, and $u_0 = 0$ is always taken as the initial iterate.

Convergence results for AAPicard-Newton are shown in figure 8, and are quite good. Convergence is achieved in all tests, and we note that there is little change between the convergence plots on the two meshes, suggesting that AAPicard is sufficiently preconditioning Newton so that convergence may be nearly mesh independent. Computing these solutions is well known to be quite difficult, as all are steady solutions at Reynolds numbers believed beyond the first bifurcation point where a natural flow would be periodic in time. Many papers exist that compute steady solutions at higher Reynolds numbers (see e.g. [4, 8] and references therein), however seemingly none of methods directly solve the steady problem on a single mesh as we do here and none are able to achieve convergence for such high Re ; other successful methods use time-stepping (or pseudo time-stepping) and try to drive the problem to a steady state, and/or continuation methods and/or various multigrid approaches.

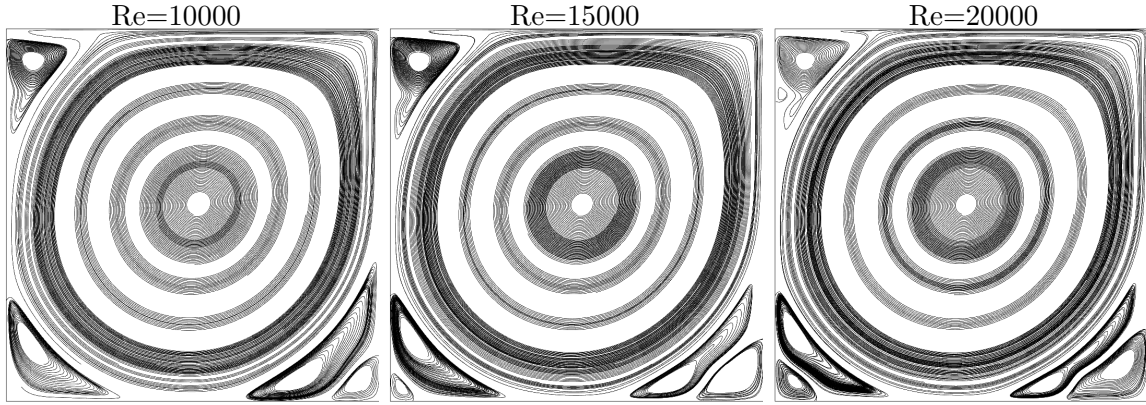


Figure 7: Shown above are streamlines of velocity solutions found for the 2D driven cavity problems with varying Re .

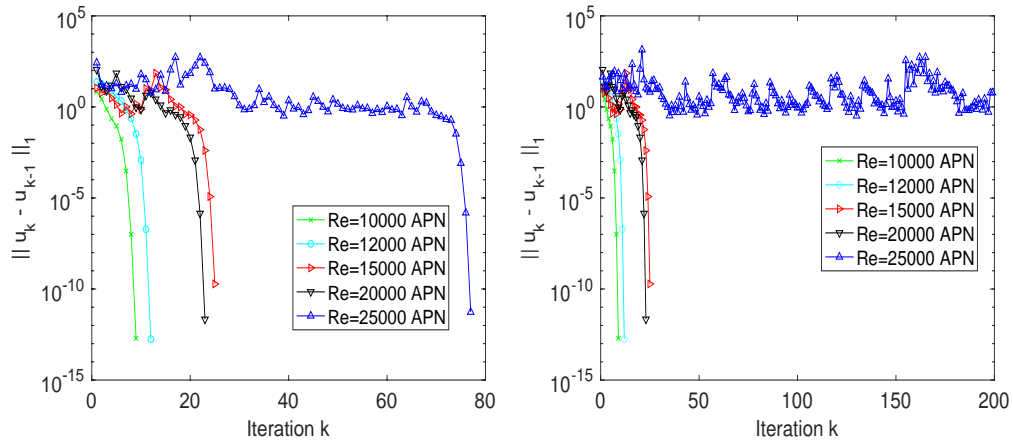


Figure 8: Shown above are convergence plots for AAPicard-Newton on a barycenter refined $\frac{1}{128}$ (left) and $\frac{1}{196}$ (right) mesh, for varying Re .

4.2.2 Channel flow past a block

The next experiment tests the proposed methods on channel flow past a block. Many studies can be found on this test, e.g. [40, 37, 38]. The domain consists of a 2.2×0.41 rectangular channel, and a block having a side length of 0.1 with center at $(0.2, 0.2)$, with the origin set to be the bottom left corner of the rectangle, see figure 9.

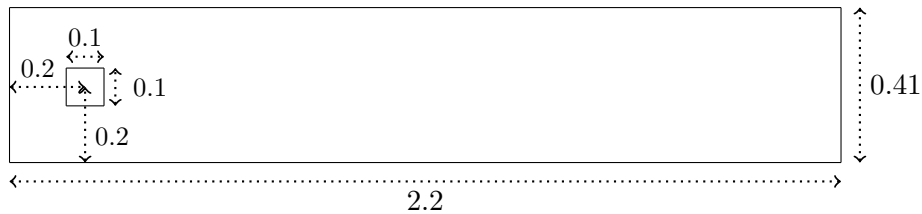


Figure 9: Shown above is the domain for the channel flow past a block numerical experiment

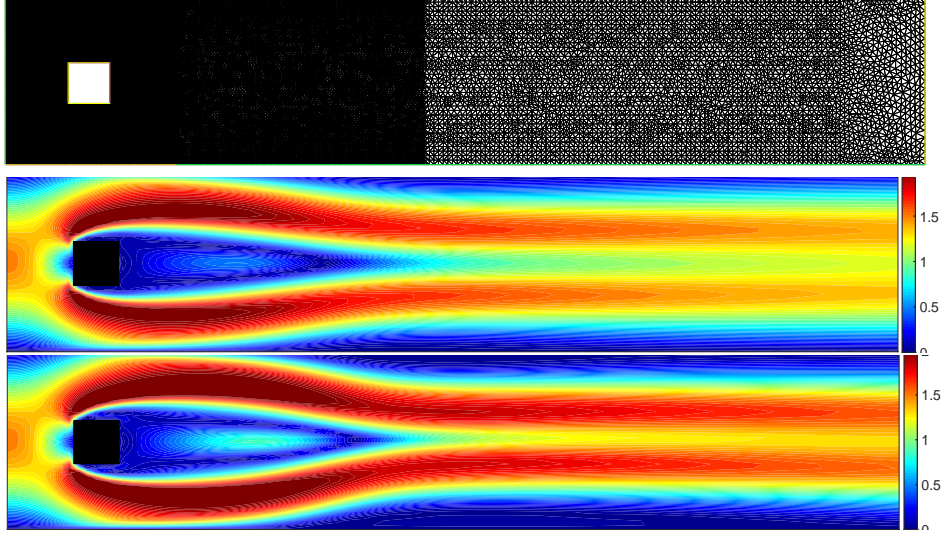


Figure 10: Shown above is the mesh used for the 2D flow past a block, before the barycenter refinement.

No-slip velocity boundary is imposed on the walls and block, and at the inflow the profile is set as

$$\begin{aligned} u_1(0, y, t) = u_1(2.2, y, t) &= \frac{6}{0.41^2} y(0.41 - y), \\ u_2(0, y, t) = u_2(2.2, y, t) &= 0. \end{aligned} \quad (4.8)$$

The outflow uses a zero traction (i.e. do nothing) homogeneous Neumann boundary condition. This problem uses no external forcing, $f = 0$. We compute with Reynolds numbers $Re = 100$ and 150 , which translate to $\nu = \frac{1}{1000}$ and $\frac{1}{1500}$ since the length scale defining the Reynolds number is taken to be the width of the block ($L=0.1$) for this problem. We note that many numerical tests have been run using $Re = 100$ and above for this test problem [40, 37, 38] and it is well known that this problem admits periodic in time solutions in this regime. Still, we search for steady solutions at these Reynolds numbers.

We compute using a mesh refined towards the left half of the channel and then refined again around the block, and finally refined again with a barycenter refinement over the entire mesh. The mesh before the barycenter refinement is applied is shown in figure 10. We compute using (P_2, P_1^{disc}) Scott-Vogelius elements, which provides 832K velocity dof and 622 pressure dof.

The Picard, Newton, Picard-Newton and AAPicard-Newton solvers are tested for both $Re = 100$ and $Re = 150$, and results are shown in figure 11. We observe that Newton fails in both cases, and in fact it essentially blows up (residual grows above 10^5 , at which point the simulation terminates). Picard converges linearly for $Re = 100$ but fails for $Re = 150$. Picard-Newton converges quickly (and quadratically) in both cases, and AAPicard-Newton provides additional speedup.

4.2.3 3D driven cavity

For our last test, we again use the 3D driven cavity benchmark problem. We use the same problem setup as above, but now test AAPicard-Newton. Results are in table 2, and we provide results

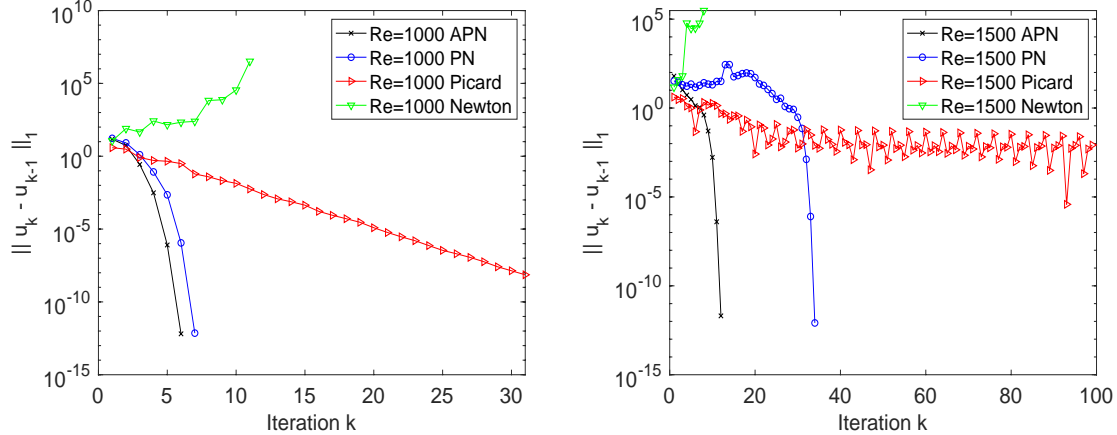


Figure 11: Shown above is the convergence for $Re=100$ and $Re=150$ for channel flow past a block, for various solvers.

from Picard-Newton (also shown above in table 1) for comparison. Here we observe mixed results from using AA: it reduced the total number of iterations, and significantly, for $Re \leq 1400$, but is unable to converge for higher Re than Picard-Newton does. In fact, Picard-Newton converges at $Re=1600$ and 1800 on mesh 3 (but not meshes 1 or 2) while AAPicard-Newton does not converge on either mesh for these Re .

	Mesh 1		Mesh 2		Mesh 3	
Re / method	P-N	AAP-N	P-N	AAP-N	P-N	AAP-N
800	7	6	9	7	9	7
1000	9	6	11	8	13	8
1200	10	7	12	10	13	10
1400	10	7	34	19	33	15
1600	11	8	F	F	68	F
1800	11	8	F	F	176	F

Table 2: Shown above are convergence results (number of iterations, ‘F’ if no convergence after 200 iterations, ‘B’ if H^1 residual grows above 10^4) for the Picard-Newton and AAPicard-Newton iterations for varying Re and on meshes 1,2, and 3.

5 Conclusions and Future Directions

We have analyzed and tested the Picard-Newton iteration for the incompressible Navier-Stokes. We have proven that this simple to implement method is locally quadratically convergent for any problem data, and has stability properties not shared by the Newton iteration: it is globally stable for problem data satisfying the uniqueness condition, and is stable at each half step for general data. Numerical tests show it is very effective on several benchmark tests, exhibiting quadratic convergence for worse initial iterates and for much higher Reynolds number than usual Newton or Picard. Moreover, even when Picard-Newton did not converge, it remained stable (as opposed to Newton, which typically blows up when it does not converge). We also considered Picard-Newton

with the Picard step enhanced with Anderson acceleration in its simplest case (depth 1 and no relaxation). Numerical results for AAPicard-Newton showed improvement over Picard-Newton, and showed a remarkable ability to converge for much higher Re than typical solvers.

Future directions include further study of Anderson acceleration applied to Picard-Newton (both application of AA to only the Picard step and to the Picard-Newton iteration itself), as well as extending the ideas to other nonlinear PDEs.

6 Acknowledgements

This material is based upon work supported by the National Science Foundation under Grant No. DMS-1929284 while the authors were in residence at the Institute for Computational and Experimental Research in Mathematics in Providence, RI, during the Acceleration and Extrapolation Methods (SP, LR and XT), and the Numerical PDEs: Analysis, Algorithms and Data Challenges (SP and LR), programs.

7 Declarations

Funding Author SP acknowledges support from the National Science Foundation from grant DMS-2011519. Author LR acknowledges support from the National Science Foundation from grant DMS-2011490.

Conflict of interest The authors have no conflicts of interest to declare that are relevant to the content of this article. The authors have no relevant financial or non-financial interests to disclose.

Code Availability The code for the current study is available from the corresponding author on reasonable request.

Availability of Data and Materials The datasets generated during and/or analyzed during the current study are available from the corresponding author on reasonable request.

References

- [1] D. Arndt, W. Bangerth, M. Bergbauer, M. Feder, M. Fehling, J. Heinz, T. Heister, L. Heltai, M. Kronbichler, M. Maier, P. Munch, J.-P. Pelteret, B. Turcksin, D. Wells, and S. Zampini. The `deal.II` library, version 9.5. *Journal of Numerical Mathematics*, 31(3):231–246, 2023.
- [2] D. Arnold and J. Qin. Quadratic velocity/linear pressure Stokes elements. In R. Vichnevetsky, D. Knight, and G. Richter, editors, *Advances in Computer Methods for Partial Differential Equations VII*, pages 28–34. IMACS, 1992.
- [3] M. Benzi and M. Olshanskii. An augmented Lagrangian-based approach to the Oseen problem. *SIAM J. Sci. Comput.*, 28:2095–2113, 2006.

- [4] L. Botti, D. Di Pietro, and J. Droniou. A hybrid high-order method for the incompressible Navier-Stokes equations based on Temam’s device. Journal of Computational Physics, 376:786–816, 2019.
- [5] P. R. Brune, M. G. Knepley, B. F. Smith, and X. Tu. Composing scalable nonlinear algebraic solvers. SIAM Review, 57(4):535–565, 2015.
- [6] T. Charnyi, T. Heister, M. Olshanskii, and L. Rebholz. On conservation laws of Navier-Stokes Galerkin discretizations. Journal of Computational Physics, 337:289–308, 2017.
- [7] X. Dai and X. Cheng. A two-grid method based on Newton iteration for the Navier-Stokes equations. Journal of Computational and Applied Mathematics, 220:566–573, 2008.
- [8] E. Erturk, T. C. Corke, and C. Gökcöl. Numerical solutions of 2d-steady incompressible driven cavity flow at high Reynolds numbers. Int. J. Numer. Methods Fluids, 48:747–774, 2005.
- [9] C. Evans, S. Pollock, L. Rebholz, and M. Xiao. A proof that Anderson acceleration improves the convergence rate in linearly converging fixed-point methods (but not in those converging quadratically). SIAM Journal on Numerical Analysis, 58:788–810, 2020.
- [10] P. Guven Geredeli, L. Rebholz, D. Vargun, and A. Zytoon. Improved convergence of the Arrow-Hurwicz iteration for the Navier-Stokes equation via grad-div stabilization and Anderson acceleration. Journal of Computational and Applied Mathematics, 422(114920):1–16, 2023.
- [11] V. Girault and P.-A. Raviart. Finite element methods for Navier-Stokes equations: Theory and Algorithms. Springer-Verlag, 1986.
- [12] P. Gresho and R. Sani. Incompressible Flow and the Finite Element Method, volume 2. Wiley, 1998.
- [13] M. Gunzburger and J. Peterson. On conforming finite element methods for the inhomogenous Navier-Stokes equations. Numer. Math., 42:173–194, 1983.
- [14] Y. He and J. Li. Convergence of three iterative methods based on the finite element discretization for the stationary Navier-Stokes equations. Computer Methods in Applied Mechanics and Engineering, 198:1351–1359, 2009.
- [15] Y. He and A. Wang. A simplified two-level method for the steady Navier-Stokes equations. Computer Methods in Applied Mechanics and Engineering, 197(17-18):1568–1576, 2008.
- [16] F. Hecht. New development in freefem++. J. Numer. Math., 20(3-4):251–265, 2012.
- [17] T. Heister and G. Rapin. Efficient augmented Lagrangian-type preconditioning for the Oseen problem using grad-div stabilization. Int. J. Numer. Meth. Fluids, 71:118–134, 2013.
- [18] V. John. Finite Element Methods for Incompressible Flow Problems. Springer, Berlin, 2016.
- [19] S. Kaya, W. Layton, and B. Riviere. Subgrid stabilized defect correction methods for the Navier-Stokes equations. SIAM Journal on Numerical Analysis, 44:1639–1654, 2006.

- [20] W. Layton. An Introduction to the Numerical Analysis of Viscous Incompressible Flows. SIAM, Philadelphia, 2008.
- [21] W. Layton, H. K. Lee, and J. Peterson. Numerical solution of the stationary Navier-Stokes equations using a multilevel finite element method. SIAM J. Sci. Comput., 20(1):1–12 (electronic), 1998.
- [22] W. Layton, H.K. Lee, and J. Peterson. A defect-correction method for the incompressible Navier-Stokes equations. Applied Mathematics and Computation, 129:1–19, 2002.
- [23] W. Layton and H. Lenferink. Two level picard and modified picard methods for the Navier-Stokes equations. Applied Mathematics and Computation, 63:263–274, 1995.
- [24] W. Layton and H. W. J. Lenferink. A multilevel mesh independence principle for the Navier-Stokes equations. SIAM J. Numer. Anal., 33(1):17–30, 1996.
- [25] X. Li, E. Hawkins, L. Rebholz, and D. Vargun. Accelerating and enabling convergence of non-linear solvers for Navier-Stokes equations by continuous data assimilation. Computer Methods in Applied Mechanics and Engineering, 416:1–17, 2023.
- [26] J. Liu, L. Rebholz, and M. Xiao. Acceleration of algebraic splitting iterations for nonlinear saddle point problems. Mathematical Methods in the Applied Sciences, pages 1–24, 2023.
- [27] K. Lust, D. Roose, A. Spence, and A. Champneys. An adaptive Newton-Picard algorithm with subspace iteration for computing periodic solutions. SIAM Journal on Scientific Computing, 19:1188–1209, 1998.
- [28] M. Mohammadi, S. Vakili-pour, and S. Ormiston. Newton linearization of the Navier-Stokes equations for flow computations using a fully coupled finite volume method. Applied Mathematics and Computation, 397(125916), 2021.
- [29] M. Olshanskii and L. Rebholz. Longer time accuracy for incompressible Navier-Stokes simulations with the EMAC formulation. Computer Methods in Applied Mechanics and Engineering, 372(113369):1–17, 2020.
- [30] C. Paniconi and M. Putti. A comparison of Picard and Newton iteration in the numerical solution of multidimensional variably saturated flow problems. Water Resources Research, 30(12):3357–3374, 1994.
- [31] S. Pollock and L. Rebholz. Anderson acceleration for contractive and noncontractive operators. IMA Journal of Numerical Analysis, 41(4):2841–2872, 01 2021.
- [32] S. Pollock and L. Rebholz. Filtering for Anderson acceleration. SIAM Journal on Scientific Computing, 45(4):A1571–A1590, 2023.
- [33] S. Pollock, L. Rebholz, and M. Xiao. Anderson-accelerated convergence of Picard iterations for incompressible Navier-Stokes equations. SIAM Journal on Numerical Analysis, 57:615–637, 2019.

- [34] A. Potschka, M. Mommer, J. Schloder, and H. Bock. Newton-Picard-based preconditioning for linear-quadratic optimization problems with time-periodic parabolic PDE constraints. SIAM Journal on Scientific Computing, 34:A1214–A1239, 2012.
- [35] L. Rebholz, A. Viguierie, and M. Xiao. Efficient nonlinear iteration schemes based on algebraic splitting for the incompressible Navier-Stokes equations. Mathematics of Computation, 88:1533–1557, 2019.
- [36] L. Rebholz and M. Xiao. The effect of Anderson acceleration on superlinear and sublinear convergence. Journal of Scientific Computing, 96(34), 2023.
- [37] W. Rodi. Comparison of LES and RANS calculations of the flow around bluff bodies. Journal of Wind Engineering and Industrial Aerodynamics, 69-71:55–75, 1997. Proceedings of the 3rd International Colloquium on Bluff Body Aerodynamics and Applications.
- [38] A. Sohankar, L. Davidson, and C. Norberg. Large Eddy Simulation of Flow Past a Square Cylinder: Comparison of Different Subgrid Scale Models . Journal of Fluids Engineering, 122(1):39–47, 11 1999.
- [39] R. Temam. Navier-Stokes equations. Elsevier, North-Holland, 1991.
- [40] F.X. Trias, A. Gorobets, and A. Oliva. Turbulent flow around a square cylinder at Reynolds number 22,000: A DNS study. Computers & Fluids, 123:87–98, 2015.
- [41] K.L. Wong and A.J. Baker. A 3D incompressible Navier–Stokes velocity–vorticity weak form finite element algorithm. International Journal for Numerical Methods in Fluids, 38(2):99–123, 2002.
- [42] M. Xiao. Superlinear convergence of Anderson accelerated Newton’s method for solving stationary Navier-Stokes equations. Numerical Methods for Partial Differential Equations, 39(4):3089–3107, 2023.
- [43] J. Zhang. A relaxed Newton-Picard like method for huber variant of total variation based image restoration. Computers and Mathematics with Applications, 78(1):224–239, 2019.
- [44] S. Zhang. A new family of stable mixed finite elements for the 3D Stokes equations. Mathematics of Computation, 74(250):543–554, 2005.